EVALUATION OF HIGH-RESOLUTION SEA SURFACE CURRENT FIELDS IN THE BALTIC SEA DERIVED FROM MULTI-SENSOR SATELLITE IMAGERY

Benjamin Seppke[(1)], Martin Gade[(2)], and Leonie Dreschler-Fischer[(1)]

[(1)] Universität Hamburg, Department Informatik, Cognitive Systems Laboratory, Hamburg, Germany, E-mail: {seppke, dreschler}@informatik.uni-hamburg.de
[(2)] Universität Hamburg, Zentrum für Meeres- und Klimaforschung, Institut für Meereskunde, Hamburg, Germany, E-mail: martin.gade@zmaw..de

ABSTRACT

We present evaluations of two-dimensional surface current fields based on quantitative comparisons of satellite images with numerical model results provided by the German Federal Maritime and Hydrographic Agency (BSH). Earlier studies have shown that multi-sensor data can be used to derive sea surface. However, a quantitative evaluation of the resulting vector fields is difficult, due to the low availability of in-situ measurements. Current predictions made by numerical models are of higher resolution, but still below the resolution of the computed currents. Additionally, they predict the currents for coarser water-depth intervals rather than the currents on the very surface. Thus, we explore different spatial interpolation methods and present the resulting comparisons.

1. INTRODUCTION

Mesoscale dynamic sea surface features, such as eddies, fronts, or dipoles, are of key importance for our understanding of local dynamics of the marine coastal environment. Series of satellite images can be used to compute sea surface currents, because natural and man-made surface films affect the sea surface and thus are visible on satellite imagery.

In recent studies we have shown that pairs of remote sensing images from different space-borne sensors can be used to derive sea surface current fields, if there are features visible on both images that are driven by the local surface motion (see [3]). The satellite images are not restricted to a certain resolution, but need to be acquired within a short time period (from less than an hour to a day, depending on the local currents and on the dynamic features to be resolved).

According to the different methods for sea surface current derivation (see [8]), different error sources exist. Additionally, "ground truth" for computed high-resolution current fields is rare, because of the sparsely available floating devices and the high resolution of the computed vector fields. Thus, we decided to compare our results with predictions made by numerical models (v2 and v3) of the German federal Maritime and Hydrographic Agency, BSH. More information about the models can be found in [5].

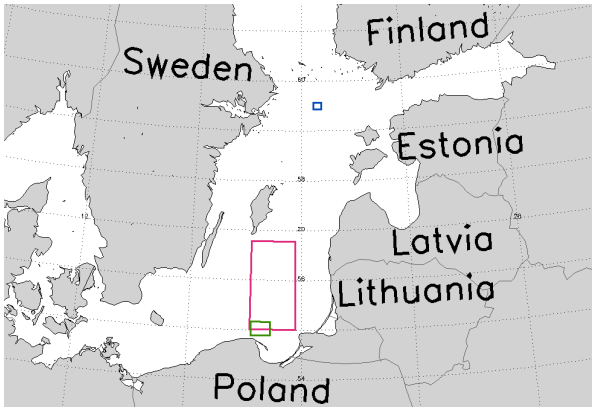

Figure 1: A map of the Baltic Sea showing the different regions of interest used for this paper. First case (blue), second case (red), and third case (green)

To perform a quantitative comparison between the computed sea surface currents, we will explore different interpolation strategies and see how the error evolves with respect to the main quality or process-parameter. Our aim is to analyze comparison methods, which allow for an automatic or user assisted evaluation of computed high-resolution sea surface current fields using model data. These evaluations could then be determined (semi-) automatically for each computed current field to describe the quality with respect to the model data.

2. SATELLITE DATA

We have selected three examples comparing currents computed from signatures of sea surface films imaged by different sensors, both for single- and multi-sensor cases, with model results.

The first case, shows images of multiple sensors: the Thematic Mapper (TM), the ERS2 Synthetic Aperture Radar (SAR) during extensive summer algae (cyanobacterial) blooms in July 1997 (Northern Baltic Proper). These images were taken with a time lag of about one hour and were processed at a spatial resolution of 30m per pixel.

For the second case, we present the computation of large-scale current fields. This does not require high-resolution satellite data, but rather images with a large spatial coverage at a lower spatial and temporal resolution. Again, the images show natural films on the

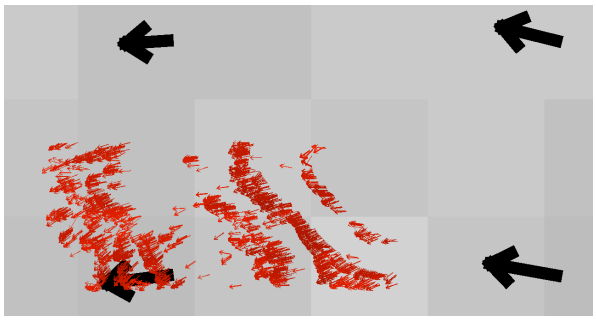

Figure 2: Computed sea surface currents (red) and sea surface currents predicted by the BSH v2 model (black) for the first case. The computation of currents was performed using a feature based fast maximum cross-correlation.

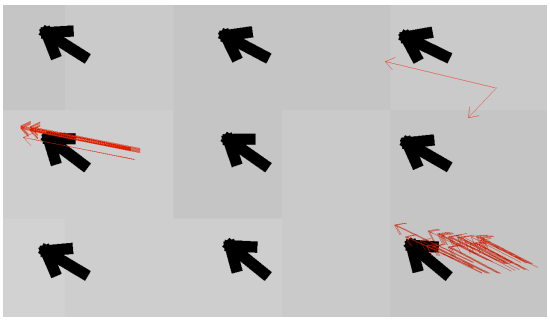

Figure 4: Computed sea surface currents (red) and sea surface currents predicted by the BSH v3 model (black) for the third case. The computation of currents was performed using a feature based fast maximum cross-correlation.

sea surface. We used a pair of Sea-viewing Wide Field-of-view Sensor (SeaWiFS) images acquired in August 1999 during algae (cyanobacterial) blooms in the Southern Baltic Proper. The time lag between the images was about 24 hours and they were processed at a spatial resolution of 1.1km per pixel.

For the third case, we show that singular man-made features on high-resolution satellite imagery, such as oil spills visible on SAR images, can be used to derive local currents. The pair of images we used for this case were taken by the ENVISAT Advanced SAR after an oil spillage north of the Bay of Gdansk in May 2005. The spatial image resolution is 150m per pixel, and the images were taken within about 11 hours

3. CURRENT DERIVATION

The basic requirement for the use of satellite data for motion detection is that both natural and man-made surface films affect the sea surface and thus are visible on satellite imagery (both optical and microwave data). Hence, using different image processing techniques we are able to compute high-resolution sea surface current fields from these current tracers.

For the first case (see Fig. 2), we used a feature-based (local) method, which is based on a fast maximum cross-correlation with an a priori determination of a global scene motion (see [2, 5]). This results in a sparse sea surface current vector field with an assigned correlation value for each vector.

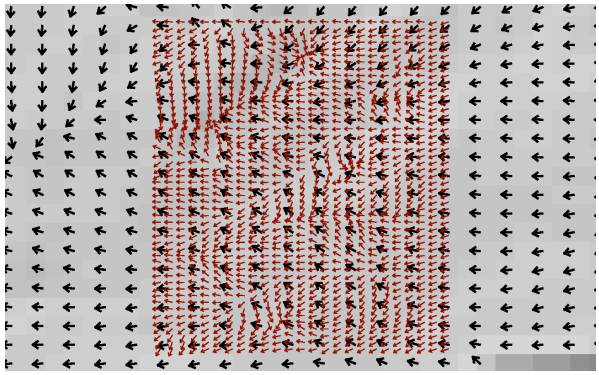

Figure 3: Computed sea surface currents (red) and sea surface currents predicted by the BSH v3 model (black) for the second case.

For the second case (see Fig. 3), we used a gradient-based (global) Optical Flow approach based on the algorithm proposed by Horn & Schunck (see [4]). This algorithm results in a dense sea surface current vector field, without assigned quality measurements. Note that not all vectors of the computed current vector field are displayed in Fig. 3. We only display a subset to avoid vector overlays.

For the third case (see Fig. 4), we used a feature-based maximum (normalized) cross-correlation method. However, due to the large motion and deformation of the two images oil spills, we were not able to apply the global motion estimation for this case. The resulting sea surface current vector field is even sparser than the vector field we derived for the second case because of the few features (boundaries of each oil spill) that have been used for tracking.

From the resulting vector fields (see Fig. 2, Fig. 3, and Fig. 4), we see that all computed currents (red) are of higher resolution than the model predictions (black). As the Optical Flow algorithm does not assign a quality measure, we cannot analyze or evaluate the current fields equally for all three cases: We have to find methods for both, the (correlation coefficient) weighted sparse and the non-weighted dense case.

4. COMPARISON METHODS

In this paper we present evaluations of the two-dimensional surface current fields based on quantitative comparisons with numerical model results provided by the local hydrographic agency BSH.

Due to the fact that the model results are of lower resolution, and have been calculated for a wider range of water depths, we have to choose adequate comparison methods. Both the BSH v2 and the BSH v3 model predict surface currents for an upper layer of 0-8m, whereas our currents are derived for the topmost

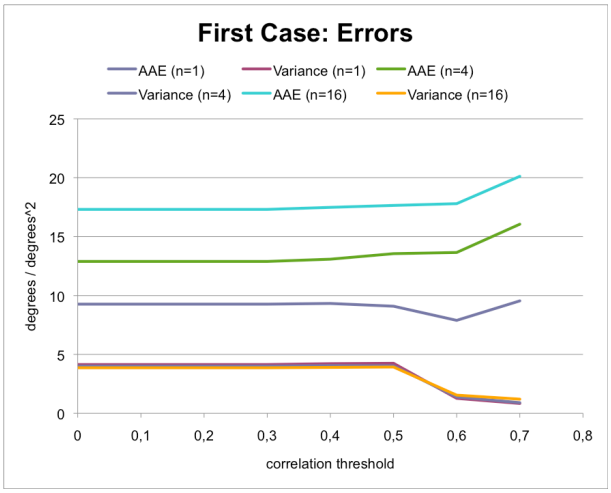

Figure 5: Error analysis for the first case. The average angular errors (AAE) and its variance are plotted for different interpolation methods (n nearest neighbors for interpolation) and different minimum correlation coefficients.

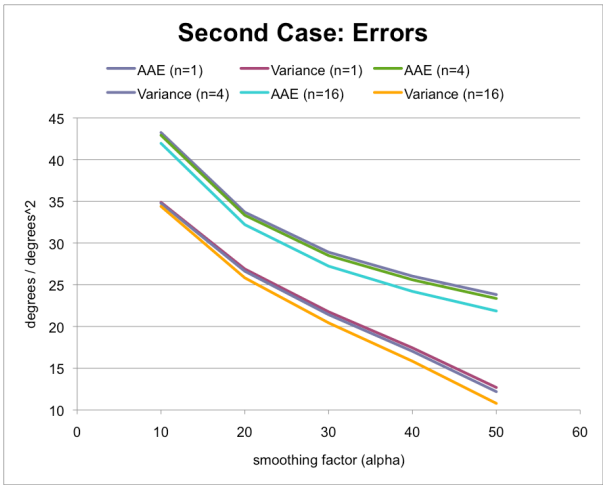

Figure 6: Error analysis for the second case. The average angular errors (AAE) and its variance are plotted for different interpolation methods and different smoothing factors of the Optical Flow algorithm.

centimeters of the sea surface. Instead of trying to correct for this, we compared the computed sea surface currents and the model currents of the uppermost layer.

We performed an interpolation of the model vectors (using the 1, 4, and 16 nearest model vectors) for each computed current vector to compare the computed currents with respect to their angular divergence. This can be seen as a smoothness assumption between the gaps of the model vectors. Note that this is only one possibility for the determination of model comparison vectors. Some other interpolation strategies have been analyzed in [7].

We used an inverted distance-weighted method driven with a variable number of nearest points used for the interpolation. Thus, selecting only one nearest point results in a nearest neighbor interpolation, selecting four points results in a bilinear interpolation, etc. After the interpolation of the model currents we determined the average angular error (*AAE*) and its variance between the computed currents and the interpolated model currents. The *AAE* of two vector fields, VF_1 and VF_2, is defined as:

$$AAE(VF_1, VF_2) = \frac{1}{|dom(VF_1)|} \sum_{i \in dom(VF_1)} \left| a\cos\left(\frac{VF_1(i) \cdot VF_2(i)}{\|VF_1(i)\| * \|VF_2(i)\|} \right) \right| \qquad (1)$$

where *VF(i)* denotes a vector of a vector field *VF* at position *i*. The variance of the *AAE* is defined analogously. The *AAE* has already proven to be a good comparison method for the result of different motion estimation algorithms, especially for the comparison of the results of Optical Flow algorithm with computer generated (rendered) sequences (see [1]).

5. RESULTS

Due to the differences in the derivation technique of the sea surface current fields and the different sensors that were used, we present results of the comparisons separately in the consequent subchapters.

5.1. First Case: Natural Films Imaged by Multiple Sensors

For the first case, we explore the dependency between the AAE and the correlation coefficient for a selection of different nearest neighbors used for the interpolation of the model data. We introduce the correlation threshold operation of a (correlation coefficient) weighted vector field, which systematically filters out vectors of low correlation. A correlation threshold of e.g. 0.3 applied to a vector field results in a vector field where all vectors with a correlation below 0.3 are filtered out. In addition to the error, we also calculated its variance.

As shown in Fig. 5, the errors decrease with an increasing correlation threshold, until there are too few currents left to allow stable statistics. We found, that the few derived currents with the highest correlation coefficients vary from the model results more than the others. This may explain the small increase at high correlation coefficients (Fig. 5). However, the error remains small (below 10.0°, when using a single neighbor interpolation of the model data).

5.2. Second Case: Natural Films Imaged by a Single Sensor (SeaWiFS)

The results of the second case need to be evaluated differently because the currents were derived using an Optical Flow algorithm and thus are dense and non-weighted. We investigated the dependency between the

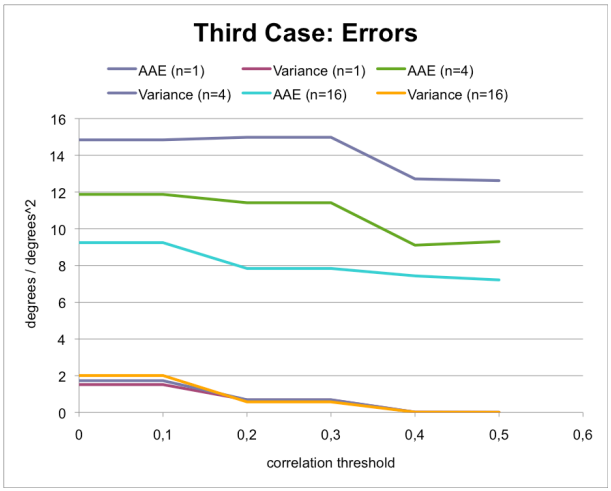

Figure 7: Error analysis for the third case. The average angular errors (AAE) and its variance are plotted for different interpolation methods and different minimum correlation coefficients.

AAE and the smoothing factor (alpha) of the Optical Flow algorithm (see Fig. 6). Under the assumption that the modeled sea surface currents are smooth the *AAE* decreases with increasing smoothing factor of the Optical Flow algorithm. Moreover, the variance of the *AAE* is also decreasing, which indicates that smaller turbulent structures are smoothed out.
Note that in general, the error values for this case are higher due to the small-scale turbulent structures (eddies) that were computed from the SeaWiFS data, but do not occur in the model currents.

5.3. Third Case: Man-Made Films Imaged by a Single Sensor (SAR)

For the third case, we performed an error analysis based on the same parameters, which we have used for the first case. Again, we see how the errors decrease for an increasing correlation threshold. Unlike the first case, the few derived currents with the highest correlation values do neither differ from the others nor from the model predicted currents. Another difference of the error analysis between the first and third case is the amount of the error with respect to the number of neighbors, which have been used for interpolation. For the third case the quality improves with increasing neighbors. This is caused by the model current field, which predicts distant currents that are more similar to the computed currents in the direct neighborhood. However, the error remains small (below 14.0° when using nearest-neighbor interpolation of the model data) for correlation coefficients greater than 0.3.

6. CONCLUSIONS

In general, our results show a very good agreement between the computed currents and the model results. It is remarkable that the errors for the feature-based method are already small for low correlation coefficients. This may be due to the well working feature detection method, which allows a tracking of the natural films only. Thus, the low correlation values may correspond to larger structural change of the features between both acquisitions.
The results also show that a single nearest-neighbor interpolation of the model currents is sufficient. This is insofar advantageous, since it allows for fast comparison algorithms. The errors are mainly decreasing by increasing the smoothing factor or the correlation factor respectively. However, with this increasing quality, the sparse vector field of the first case becomes sparser and the dense vector field of the second case becomes smoother. This can be interpreted as reduced information content of the computed current contrary to the decreasing AAE when compared with the model data. Another problem is the occurrence of smaller turbulent structures in the computed (Optical Flow) results, which do not occur in the model predictions. They lead to a relatively high AAE and make the interpretation of the comparison results more difficult.
On the one hand, the proposed evaluation method gives a good impression of the quality of computed currents, which may assist in the automatic quality control in further studies. On the other hand, we hope that the computed currents lead to a better understanding of mesoscale sea-surface dynamics and will help to improve the models in future.

7. ACKNOWLEDGEMENTS

Thanks are due to Hartmut Komo of the German BSH for providing the model data, and to Olga Lavrova of the Russian IKI for her help identifying the ASAR images showing oil spills.

REFERENCES

[1] Barron, J. L., Fleet, D. L., Steven S. Beauchemin, S. S., 1994, Performance of optical flow techniques. International Journal of Computer Vision 12(1): 43-77

[2] Emery, W.J., A.C. Thomson, M.J. Collins, W.R. Crawford, and D.L Mackas, 1986: An objective method for computing advective surface velocities from sequential infrared satellite images. J. Geophys. Res., 91, 12 865-12 878.

[3] Gade, M., Rud, O. and Ishii, M., 1998, Monitoring algae blooms in the Baltic Sea by using spaceborne optical and microwave sensors. Geoscience and Remote Sensing Symposium Proceedings, 1998. IGARSS '98. 1998 IEEE International 2, pp. 754–756.

[4] Horn, B.K.P., and Schunck, B.G., 1981. "Determining Optical Flow". Art. Intell., 17, pp. 185-189.

[5] Kleine, E., 1994. Das operationelle Model des BSH fur Nordsee und Ostsee, Konzeption und Übersicht. Technical report, Bundesamt fur Seeschiffahrt und Hydrographie. Hamburg.

[6] Lewis, J. P., 1995. Fast Normalized Cross-Correlation. In: Vision Interface, Canadian Image Processing and Pattern Recognition Society, pp. 120–123.

[7] Mark, S., 2009. Entwicklung eines Werkzeuges zur Messung der Genauigkeit von Bewegungsfeldern der Meeresoberfläche, Diploma Thesis, Dept. Informatik, University of Hamburg

[8] Seppke, B., Gade, M., and Dreschler-Fischer, L., 2009. Sea Surface Current Fields in the Baltic Sea Derived From Multi-Sensor Satellite Data. Proceedings of the ISPRS Hannover Workshop 2009